

# Neuromorphic Encoding / Reconstruction of Images Represented by Poisson Counts

V. E. Antsiperov <sup>a</sup>

*Kotelnikov Institute of Radioengineering and Electronics of RAS, Mokhovaya 11-7, Moscow, Russian Federation*

**Keywords:** Neuromorphic Systems, Poisson Counts, Sampling Representation, Receptive Fields, Lateral Inhibition, Poisson Disorder Problem, Colour Constancy, Retinex, Edge-Directed Interpolation, Perceptual Quality.

**Abstract:** The paper discusses one of the possible neuromorphic methods for processing relatively large volumes of streaming data. The method is mainly motivated by the known mechanisms of sensory perception of living systems, in particular, methods of visual perception. In this regard, the main provisions of the method are discussed in the context of problems of encoding/recovering images on the periphery of the visual system. The proposed method is focused on representing input data in the form of a stream of discrete events (counts), like the firing events of retinal neurons. For these purposes, a special representation of data streams is used in the form of a controlled size samples of counts (sampling representations). Based on the specifics of the sampling representation, the generative data model is naturally formalized in the form of a system of components distributed over the field of view. These components are equipped with some “neuromorphic” structure, which model a system of receptive fields, embodying universal principles (including lateral inhibition) of the neural network of the brain. The mechanism of lateral inhibition is implemented in the model in the form of an antagonistic structure of the RF centre / surround. Issues of image decoding are considered in the context of restoring spatial contrasts, which partly emulates the work of the so-called simple / complex cells of the primary visual cortex. It is shown that the model of coupled ON-OFF decoding allows for the restoration of sharp image details in the form of emphasizing edges.


## 1 INTRODUCTION

Digital technologies are represented today in almost all spheres of human activity. The use of digital data on the platform of modern computer technologies provides unique opportunities for using existing knowledge, generalizing knowledge in the form of generative models, synthesizing, and implementing optimal methods for processing and analyzing data, including digital images data.

With the advent of powerful and cheap computer technologies at the turn of the 20th–21st centuries, it turned out to be possible to significantly expand the arsenal of data models used, guided not so much by the issues of approximating them with classical statistical schemes, but by the specific features of the data themselves. New possibilities for aggregation in computer storage/servers of large volumes of data also contributed to the diversification of models. This trend has resulted in revolutionary advances in

machine learning and a few deep learning approaches based on artificial neural networks (Nguyen, 2019).

Unfortunately, the heyday of current artificial neural networks does not promise to be long. The problem is that existing neural network applications are implemented on computers with von Neumann computing architecture. Since they store program and data blocks in shared memory space, this implies a continuous, intensive exchange of information between the memory and the processor. Considering that the next generation of computer technology will be focused on performing  $\sim 10^{18}$  flops, they, with all their incredible power, will consume 20~30 megawatts of power if they continue to be based on the traditional architecture. Neither Moore's doubling law, nor Dennard's scaling law, which until recently ensured an increase in the productivity of computer technology, will be able to overcome the difficulties associated with fundamentally physical (thermodynamic) limitations.

<sup>a</sup>  <https://orcid.org/0000-0002-6770-1317>

One of the promising ways to solve this problem seems to be the transition to the use of neuromorphic computing systems based on the principles of the human brain (Christensen, (2022)). Their most attractive features are the principles of biological neural networks, such as highly parallel information processing, processing procedures embedded directly in data blocks, scalability, event-driven calculations, etc. It is expected that a new generation of computers based on these principles (sometimes called third-generation neural – spiking networks) can be effectively used both for storing extremely large volumes of data and for processing it in an acceptable time and at the same time with much less energy consumption. In addition to energy efficiency, neuromorphic systems are ideal for implementing machine learning approaches and have enormous potential for computing beyond the von Neumann paradigm. These advantages will give them priority in most information technologies.

Considering this, we have recently made attempts to initiate the research on the development of new methods for working with data streams based on the principles of neuromorphic computing (Antsiperov, 2022). The proposed work presents some of the results of the efforts undertaken. Namely, below we discuss the possibilities of processing relatively large volumes of streaming data using neuromorphic methods in the problem of image encoding / restoration. The proposed methods are focused on representing input data in the form of a stream of discrete events (counts), like the firing events of retinal neurons. For its adequate statistical description, a special representation was developed in the form of sample of counts (sampling representation). The probabilistic nature of the representation naturally leads to a generative model of the streaming data encoder, which can be formalized as a parametric model of a set (mixture) of components. We discovered that within the proposed generative model the search for optimal encoding can be reformulated as a statistical maximum likelihood problem. We solved this ML problem under the assumption that a set of components has a receptive field (RF) structure that embody universal principles (including lateral inhibition) of a biological neural network. Issues of image decoding are considered in the context of restoring spatial contrasts, which also partly emulates the work of the so-called simple / complex cells of the primary visual cortex. It is shown that the coupled ON-OFF decoding model allows for the restoration of sharp image details in the form of edge-directed interpolation.

The main content of the work is grouped in the following three sections. Section 2 contains a brief overview of neurophysiological data on the structure of RFs and methods for it modelling. Section 3 is related to the substantiation of the statistical description of the RF functions for processing the input stream of samples. And in the last section the results of the numerical procedure for image restoration (decoding) are discussed based on the results of encoding the input stream by the RF system. The conclusion briefly summarizes the results and outlines avenues for further research.

## 2 RETINAL RECEPTIVE FIELDS AS STRUCTURAL UNITS OF EDGE ENCODING

As mentioned above, the proposed encoding method deals with equipping the image forming area with some fixed “neuromorphic” structure. It is believed that this structure is initially given and does not depend, among other things, on the radiation intensity focused by the lens of the eye on the retina, or by the optics of the video camera on the CMOS-matrix. Essentially, the structure mentioned is simple enough. Namely, it models the structure of the receptors (outer) layer of the human (or higher vertebrates) retina, known as the receptive field (RF) system.

The general concept of RFs as structural units of sensory neuronal systems of living organisms has been known for a long time. As for the periphery of the visual system, the beginning of systematic research and analysis of the RF features is usually associated with the work of Kuffler (Kuffler, 1953) in the early 50s. According to the tradition, that followed Kuffler, receptive fields are understood as small areas of the retina containing tens to hundreds of input receptors (cones/rods), whose stimulation leads to the activation of certain output neurons (RGCs - retinal ganglion cells). It is important to note that along the path of data propagation from receptors to the RGC, visual information undergoes several transformations and modifications carried out by intermediate neurons (horizontal, bipolar and amacrine cells) of the retina. As a result, in addition to the spatial structure, the RFs also has a certain functional arsenal. It is associated with the division of the RF surface into two parts: a central region that receives data directly from the retinal receptors, which is called the RF-centre, and a peripheral region concentric to the centre, which receives data through horizontal cells and is called the RF-surround. It is

usually believed that the ratio of the centre size to the size of the RF is on average  $\sim 1:1.6$  (Marr, 1980). Note that the size of the RFs can vary significantly depending on the location of the RF relative to the centre part of the retina (fovea) – from fractions of degrees of visual angle to several degrees (angle of  $1^\circ$  on the retina  $\sim 0.3$  mm, on the external screen at the best distance vision (at 60 cm)  $1^\circ \sim 1$  cm) (Bear, 2007).

Kuffler (Kuffler, 1953) also found that the types of RFs that differ in their response to illumination contrast are closely related to the functional structure. ON-type fields are activated (depolarized) when a small spot of light is projected onto their centre. Conversely, OFF-type fields are activated when their centre is slightly darkened. It should be stressed that the reactions of both types of cells are cancelled with simultaneous stimulation of the centre and the surround (Bear, 2007). Due to this the centre / surround of the RF constitutes an antagonistic pair (structure). One consequence of this is that most retinal RGCs respond weakly to slow (on the RF scale) illuminance changes across the entire retina, but respond markedly to sharp illuminance contrasts within a surface of individual RF.

Let us formalize the presented neurobiological facts in the form of a simple model, which will reflect the main RF functionality and at the same time find out what the minimum set of assumptions is required for this. Let us denote by  $\Omega$  the flat image forming region with coordinates  $\vec{x} = (x_1, x_2)$ . Let the image correspond to the recorded radiation intensity  $I(\vec{x})$  on  $\Omega$ . As a RF, we consider the region  $\Delta \subset \Omega$  of the area  $\sigma$ , consisting of the centre  $\Delta_c \subset \Delta$  of the area  $\sigma_c$  and the concentric surround  $\Delta_s \subset \Delta$  of the area  $\sigma_s$ , so that  $\Delta_c \cup \Delta_s = \Delta$ ,  $\Delta_c \cap \Delta_s = \emptyset$ ,  $\rightarrow \sigma_c + \sigma_s = \sigma$ . Thus, regions  $\Delta_c$  and  $\Delta_s$  represent a partition of RF  $\Delta$ , as shown in Figure 1 (A).

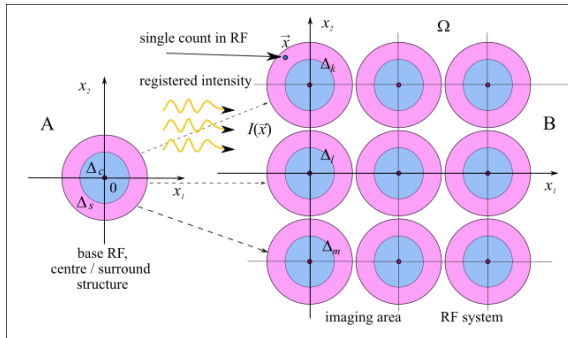


Figure 1: Schematic representation of the single typical RF and the corresponding RF system. (A) RF with centre / surround structure, (B) homogeneous RF system with typical RFs at the nodes of squared grid covering image  $\Omega$ .

Let us introduce the values of the average intensities  $\bar{I}$ ,  $\bar{I}_c$ ,  $\bar{I}_s$  corresponding, respectively, to the RF, to its centre and to its surround:

$$\begin{aligned} \bar{I} &= \frac{1}{\sigma} \iint_{\Delta} I(\vec{x}) ds, \\ \bar{I}_c &= \frac{1}{\sigma_c} \iint_{\Delta_c} I(\vec{x}) ds, \quad \bar{I}_s = \frac{1}{\sigma_s} \iint_{\Delta_s} I(\vec{x}) ds. \end{aligned} \quad (1)$$

Let us choose a point in the RF region, for example, coinciding with its centre of gravity  $\vec{X}_\Delta = \iint_{\Delta} \vec{x} ds / \sigma$ , and expand the intensity  $I(\vec{x})$  at this point into the Taylor series up to powers  $(\vec{x} - \vec{X}_\Delta)$  of the second order inclusive ( $T$  is transpose sign):

$$\begin{aligned} I(\vec{x}) &\approx I(\vec{X}_\Delta) + [\vec{\nabla}^T I(\vec{X}_\Delta)](\vec{x} - \vec{X}_\Delta) + \\ &+ \frac{1}{2} (\vec{x} - \vec{X}_\Delta)^T [\vec{\nabla} \vec{\nabla}^T I(\vec{X}_\Delta)] (\vec{x} - \vec{X}_\Delta). \end{aligned} \quad (2)$$

Substituting approximation (2) into equation (1) for  $\bar{I}$ , we obtain (iff  $\vec{X}_\Delta$  is the centre of gravity of  $\Delta$ ):

$$\bar{I} \approx I(\vec{X}_\Delta) + \frac{1}{2} Sp(\vec{\nabla} \vec{\nabla}^T I(\vec{X}_\Delta) \times \hat{Y}_\Delta), \quad (3)$$

where  $Sp(\dots)$  is the trace of a matrix and

$$\hat{Y}_\Delta = \frac{1}{\sigma} \iint_{\Delta} (\vec{x} - \vec{X}_\Delta)(\vec{x} - \vec{X}_\Delta)^T ds \quad (4)$$

is the matrix of the  $\Delta$ 's second moments of inertia.

Note that  $\hat{Y}_\Delta$  (4) is determined only by the geometric shape of the region  $\Delta$  and does not depend on its position (the center of gravity  $\vec{X}_\Delta$  depends).

The same reasoning can also be repeated in relation to  $\bar{I}_c$ , which will take a form like (3), where instead of  $\vec{X}_\Delta$ ,  $\hat{Y}_\Delta$  there will be the values  $\vec{X}_c$ ,  $\hat{Y}_c$ :

$$\begin{aligned} \vec{X}_c &= \frac{1}{\sigma_c} \iint_{\Delta_c} \vec{x} ds, \\ \hat{Y}_c &= \frac{1}{\sigma_c} \iint_{\Delta_c} (\vec{x} - \vec{X}_c)(\vec{x} - \vec{X}_c)^T ds. \end{aligned} \quad (5)$$

If the RF  $\Delta$  and its centre  $\Delta_c$  are located so that their centres of gravity coincide  $\vec{X}_c = \vec{X}_\Delta$ , then an important consequence follows from the obtained relations:

$$\delta \bar{I}_c = \bar{I} - \bar{I}_c = \frac{1}{2} Sp(\vec{\nabla} \vec{\nabla}^T I(\vec{X}_\Delta) \times [\hat{Y}_\Delta - \hat{Y}_c]). \quad (6)$$

A similar relation can be obtained for the difference  $\delta \bar{I}_s = \bar{I} - \bar{I}_s$ , however, it is easier to obtain it from the relationship  $\sigma_c \delta \bar{I}_c + \sigma_s \delta \bar{I}_s = 0$ , followed from (1).

For the convenience of further reasoning, it is worth choosing a coordinate system with the origin at the common centre of gravity  $\vec{X}_c = \vec{X}_\Delta = \vec{0}$ . In this case, if the centre region  $\Delta_c$  is similar to the RF region  $\Delta$ , then with a homogeneous linear transformation  $\vec{x} \rightarrow k\vec{x}$  with some  $k > 1$ , the region  $\Delta_c$  will be

mapped into  $\Delta$  and, accordingly,  $\hat{Y}_c \rightarrow k^2 \hat{Y}_c = \hat{Y}_\Delta$ . Relationship (6) in this case takes the form:

$$\delta \bar{I}_c = \bar{I} - \bar{I}_c = \frac{k^2 - 1}{2k^2} Sp(\vec{\nabla} \vec{\nabla}^T I(\vec{0}) \times \hat{Y}_\Delta). \quad (7)$$

As follows from definition (4), the matrix  $\hat{Y}_\Delta$  is symmetric and positive definite; therefore, there is an orthogonal coordinate system (of normalized eigenvectors) in which  $\hat{Y}_\Delta$  is diagonal, and the elements on the diagonal are positive and add up to the total moment of inertia  $Z = \iint_{\Delta} \vec{x}^2 ds / \sigma$ . If, moreover, the moments are equal ( $= Z/2$ ), then  $\hat{Y}_\Delta$  is a multiple of the identity matrix and (7) takes the following final form:

$$\delta \bar{I}_c = \bar{I} - \bar{I}_c = \frac{(k^2 - 1)Z}{4k^2} Sp(\vec{\nabla} \vec{\nabla}^T I(\vec{0})) = \frac{(k^2 - 1)Z}{4k^2} \Delta I(\vec{0}), \quad (8)$$

where  $\Delta$  is the Laplace operator (Laplacian).

The right-hand side of (8) can be viewed as the output at coordinates origin  $\vec{x} = \vec{0}$  of applied to the intensity  $I(\vec{x})$  Laplacian filter. This immediately suggests an analogy between the RF function, which calculates the intensity defect  $\delta \bar{I}_c = \bar{I} - \bar{I}_c$  and the Marr operator (Marr, 1980), which serves to detect edges in digital images (second order in derivatives edge detector). Marr proposed to characterize lines of sharp changes in intensity (edges) by the condition  $\Delta I(\vec{x}) = 0$ , i.e. as lines where the Laplacian of intensity intersects zero level (zero-crossings). The motivation for this choice is as follows. Let us assume that the zero-crossing line passes through the origin  $\vec{x} = \vec{0}$  and in the vicinity of the origin the intensity behaves as a step function (Haralick, 1984):

$$I(\vec{x}) \approx I(\vec{0}) + \vec{a}^T \vec{x} + S(\vec{b}^T \vec{x}), \quad (9)$$

where  $I(\vec{0})$  is the intensity at the origin,  $\vec{a}$  is some vector associated with the large-scale illumination gradient,  $\vec{b}$  is a vector associated with the normal to the step, and  $S(\dots)$  is a monotonic function of one variable like the smoothed Heaviside step function. It immediately follows from (9) that in the vicinity of the step  $\Delta I(\vec{x}) = S''(\vec{b}^T \vec{x}) \vec{b}^2$ . If we require that at the points of the line  $\vec{b}^T \vec{x} = 0$  the step intensity gradient  $S'(0) \vec{b}$  be maximum, then it is necessary that  $S''(0) = 0$ , which is equivalent to Marr condition. Thus, the edges of the step type intensity are determined by zero-crossings of the Laplacian filter  $y = \Delta I(\vec{x})$ .

In connection with the above reasoning, we note the following circumstance. In fact, from the step model of local intensity (9) not only the Marr

condition  $\Delta I(\vec{x}) = 0$  follows, but also the equality to zero of the matrix  $\vec{\nabla} \vec{\nabla}^T I(\vec{0}) = S''(0) \vec{b} \vec{b}^T$ , whose trace is the Laplacian. In this case, the necessary condition for the intensity jumps on the RF in the form  $\delta \bar{I}_c = 0$  will follow directly from (6) without additional assumptions leading to (7) or (8). Thus, for the necessity of the condition  $\delta \bar{I}_c = 0$  with a stepwise change in  $I(\vec{x})$ , it is quite sufficient that the location of the RF  $\Delta$  and its centre  $\Delta_c$  ensures the equality of their centres of gravity  $\vec{X}_c = \vec{X}_\Delta$  (equal to  $\vec{0}$  in a special coordinate system). As a result, replacing the Marr condition  $\Delta I(\vec{x}) = 0$  with the derived condition  $\delta \bar{I}_c(\vec{X}_i) = 0$ , we arrive at a more direct approach to detecting edges in the form of zero-crossings.

It is interesting to note that the defect  $\delta \bar{I}_c = \bar{I} - \bar{I}_c$  can also be considered as the output of a piecewise constant filter with a compact support in the form of a RF region  $\Delta$ . Two filter levels are positive constant  $1/\sigma$  at the surround and negative  $-\sigma_s/\sigma_c \sigma$  at the centre of the RF, so that the filter has zero-DC response. Such a filter (up to sign) was previously proposed under the name COSO (center-on-surround-off) in (Allebach, 1996). However, in this work COSO filter was proposed as an approximation of the Marr's Laplacian-of-Gaussian (LoG) filter to save computation, but not for fundamental reasons.

Although the approach described above seems attractive, until the method of its implementation has not been determined, it has only conceptual significance. In fact, it is the features of the computer implementation that determine the originality of the approach. Let us therefore consider some aspects of a possible computer implementation of the approach proposed.

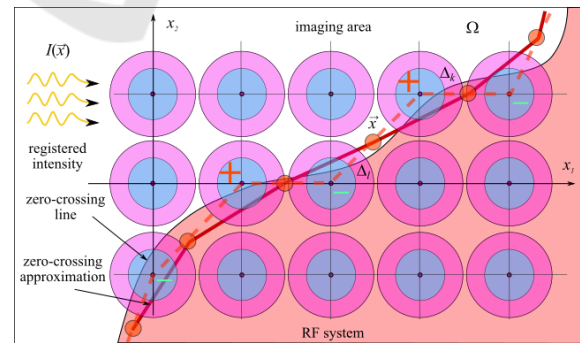


Figure 2: Marr's method for edge detection. The set of ON-fields is marked with a "+" sign, the set of OFF-fields with a "-" sign. Segments connecting the centres of the nearest ON- and OFF-fields are marked with a dotted line. Zero-points found by interpolation on these segments form a broken line – zero-crossing approximation (edge).

The first aspect is that, unlike the COSO filter (Allebach, 1996), we cannot generate values of  $\delta\bar{I}_c$  at arbitrary points  $\vec{x}$  of the image  $\Omega$ , but only at locations  $\{\vec{X}_i\}$  of a fixed discrete RF system  $\{\Delta_i\}$ . Therefore, the search for a solution to the nonlinear equation  $\delta\bar{I}_c = 0$  using standard, usually iterative, methods encounter problems. Indeed, at some iteration, the calculated approximation to the solution may not coincide with one of the RF centres  $\vec{X}_i$ , which, due to the lack of data at such a point, will not allow the search to continue. To solve this problem, Marr proposed a method that models the work of simple cells (neurons) located in the lateral geniculate nucleus (Marr, 1980). The main idea of Marr is as follows.

Let's consider a set of receptive fields with a noticeable positive defect  $\delta\bar{I}_c > 0$  and call them ON-fields. Similarly, we call the set of fields that have a negative defect  $\delta\bar{I}_c < 0$  OFF-fields, see Figure 2. Since these two sets do not intersect, they are separated by some imaginary boundary. Any two adjacent ON- and OFF-fields lying on both sides of this boundary have defects of different signs, therefore somewhere on the segment connecting them there must exist a point  $\vec{x}$  at which  $\delta\bar{I}_c(\vec{x}) = 0$ , as shown in Figure 2. The position of this point can be interpolated in any suitable way (for example, linear), if the positions  $\vec{X}_k$  and  $\vec{X}_l$  of these fields and corresponding values of their defects  $\delta\bar{I}_c(\vec{X}_k)$  and  $\delta\bar{I}_c(\vec{X}_l)$  are known. Having gone through all the pairs of fields in this way and connecting the nearest points found, we will obtain a broken zero-crossing line approximation of the required zero-crossings as shown in Figure 2.

The second aspect of the implementation is related to the issues of reliably determining the corresponding ON- and OFF-fields, i.e. with questions of confident resolution of alternatives  $\delta\bar{I}_c(\vec{X}_i) \leq 0$ . The problem here is that the recorded defects  $\delta\bar{I}_c(\vec{X}_i)$  (6) are noisy data, which, with signal-to-noise ratios  $SNR \sim 1$ , will often lead to false decisions. The solution here is to use threshold criteria of the type  $\delta\bar{I}_c(\vec{X}_i) > T$  or  $\delta\bar{I}_c(\vec{X}_i) < -T$  with some threshold  $T$ . However, this also raises many questions like how to choose a threshold, should it depend on the location  $\vec{X}_i$  of the RF or on the RF data  $\bar{I}(\vec{X}_i), \bar{I}_c(\vec{X}_i)$ , etc. Some of the listed issues for the case of Poisson counts were considered in previous works, see for example, (Antsiperov, 2023). Below we discuss the adaptation of the obtained results to current work.

### 3 IMAGE NEUROMORPHIC ENCODING BY THE RF SYSTEM

A statistical description of the image sampling representation in the form of multivariate distribution  $\rho(S_k|n, I(\vec{x}))$ ,  $S_k = (\vec{x}_1, \dots, \vec{x}_k)$  was obtained in previous works (see for example (Antsiperov, Kershner 2023) and looks as follows:

$$\rho(S_k|n, I(\vec{x})) = \prod_{i=1}^k \rho(\vec{x}_i|I(\vec{x})),$$

$$\rho(\vec{x}_i|I(\vec{x})) = \frac{I(\vec{x}_i)}{\iint_{\Omega} I(\vec{x}) ds}, \quad (10)$$

As has been shown, approximation (10) is valid when sample size  $k \ll \bar{n}$ , where  $\bar{n} = \alpha T \iint_{\Omega} I(\vec{x}) ds$  is the average total number of counts registered during exposure time  $T$  at light intensity  $I(\vec{x})$ . Parameter  $\alpha = \eta(h\nu)^{-1}$  characterizes the interaction of radiation with matter and depends on  $h\nu$  – the average energy of the incident photon and on dimensionless coefficient  $\eta$  – the quantum efficiency of detector material. It is noteworthy that distribution (10) has several useful properties giving it a universal character. (Antsiperov, Kershner 2023).

One of the important properties of (10) is that the dependence of  $\rho(\vec{x}_i|I(\vec{x}))$  on the intensity  $I(\vec{x})$  is almost trivial – it simply coincides with the value of  $I(\vec{x}_i)$  at the same point, up to the normalization constant. This makes it possible to illustrate a typical sampling representation, as well as its subsequent processing results, using ordinary bitmap images and considering their pixel values as an approximation of the recorded intensity, expressed in some arbitrary units.

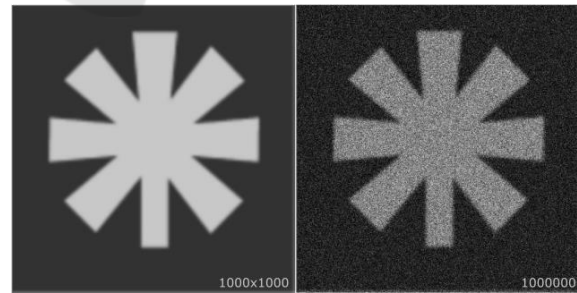


Figure 3: Illustration of the image sampling representation. On the left is the original, grayscale PNG image, on the right is its representation  $S_k$  of the size  $k = 1000000$  counts.

To illustrate a typical sampling representation for a grayscale PNG image, we generated its  $S_k$  using the Monte Carlo approach to sample from distribution of

its pixels. An image and sampling representation are shown in Figure 3. Grayscale PNG image is of size  $s \times s$ ,  $s = 1000$  pixels, color depth  $v = 8$  bits, corresponding  $S_k$  is of size  $k = 1000000$  counts. The generation of random counts was carried out by using the Monte Carlo rejection/acceptance sampling method with a uniform auxiliary distribution  $u(\vec{x}) = s^{-2}$  and constant  $M = 2^v$ .

It is easy to pass from a statistical description in preset counts (10) to description in preset local regions form (Barrett, 1997). Since the latter description (preset regions) is more suitable for the subsequent description of data associated with receptive fields, we outline its brief conclusion here.

Namely, let's take some small region  $\Delta \subset \Omega$  and consider the event of a count into it as a success, and the absence of count as a failure. According to (10), the probability of success is  $p = \iint_{\Delta} \rho(\vec{x}|I(\vec{x}))ds$ , and of failure, respectively,  $q = 1 - p$ . Then, considering the registration of count as a test in the Bernoulli scheme, we find that the probability of  $l$  out of  $k$  successes – probability of  $l$  counts of  $S_k$  in  $\Delta$  – is determined by the binomial distribution, in asymptotic  $k \gg 1$ ,  $p \rightarrow 0$ , but  $\lambda = kp = \text{const}$ , coinciding with Poissonian:

$$P_{\Delta}(l | k, p) = \frac{k!}{l!(k-l)!} p^l q^{k-l} \approx \frac{\lambda^l}{l!} \exp\{-\lambda\}, \quad (11)$$

$$\lambda = kp = k \frac{\iint_{\Delta} I(\vec{x})ds}{\iint_{\Omega} I(\vec{x})ds} = \beta \iint_{\Delta} I(\vec{x})ds,$$

where  $\beta = \alpha T k / \bar{n}$  is another parameter, however, unlike  $\alpha$  depending also on the ratio of the sampling representation  $S_k$  size to  $\bar{n}$ . For further purposes, it is convenient to express the parameter  $\lambda$  of the Poisson distribution (2) not through the registered intensity  $I(\vec{x})$ , but through the intensity of counts generated by receptors  $i(\vec{x})$ , which is proportional to the first:  $i(\vec{x}) = \beta I(\vec{x})$ . Considering this notation, the distribution of counts in  $\Delta$  (11) can be rewritten as

$$P_{\Delta}(l | i_{\Delta}) \cong \frac{(\sigma i_{\Delta})^l}{l!} \exp\{-\sigma i_{\Delta}\}, \quad (12)$$

$$i_{\Delta} = \frac{1}{\sigma} \iint_{\Delta} i(\vec{x})ds = \frac{\beta}{\sigma} \iint_{\Delta} I(\vec{x})ds,$$

where  $\sigma$  is the area of region  $\Delta$  and  $i_{\Delta}$  – the average value of intensity of counts  $i(\vec{x})$  per  $\Delta$ . Note that the mean value of  $l$ , as well as its dispersion according to the Poisson distribution (12), is exactly  $\bar{l} = \sigma i_{\Delta}$ .

Let us use the notations introduced above for a typical receptive field:  $\Delta \subset \Omega$  – the RF region of the area  $\sigma$ ,  $\Delta_c / \Delta_s$  – its centre / surround structure of areas  $\sigma_c / \sigma_s$ , respectively,  $\sigma_c + \sigma_s = \sigma$ . Let us denote the numbers of counts in the centre and in the

surround of RF by  $n_c$  and  $n_s$ . From the condition that  $\Delta_c$  and  $\Delta_s$  are the partition of  $\Delta$  it follows that  $n = n_c + n_s$  is the total number of counts on the RF. By virtue of (12), the statistical models of  $n_c$  and  $n_s$  are Poisson probability distributions:

$$n_c | i_c \sim P_c(n_c | i_c) = \frac{(\sigma_c i_c)^{n_c}}{n_c!} \exp\{-\sigma_c i_c\}, \quad (13)$$

$$n_s | i_s \sim P_s(n_s | i_s) = \frac{(\sigma_s i_s)^{n_s}}{n_s!} \exp\{-\sigma_s i_s\},$$

where  $i_c$  and  $i_s$  are the average intensities of counts in the centre and in the surround of RF:

$$i_c = \frac{1}{\sigma_c} \iint_{\Delta_c} i(\vec{x})ds, \quad i_s = \frac{1}{\sigma_s} \iint_{\Delta_s} i(x)dx \quad (14)$$

Note here that since the numbers  $n_c$  and  $n_s$  are unbiased estimates of their means  $\bar{n}_c = \sigma_c i_c$  and  $\bar{n}_s = \sigma_s i_s$ , the values  $n_c / \sigma_c$  and  $n_s / \sigma_s$  are unbiased estimates of the average intensities  $i_c$  and  $i_s$ .

Since  $n_c$  and  $n_s$  are Poisson on the disjoint regions  $\Delta_c \cap \Delta_s = \emptyset$ , they are statistically independent, and their joint probability distribution can be written as:

$$P(n_c, n_s | i_c, i_s) = P_c(n_c | i_c) P_s(n_s | i_s) = \frac{(\sigma_c i_c)^{n_c} (\sigma_s i_s)^{n_s}}{n_c! n_s!} \exp\{-[\sigma_c i_c + \sigma_s i_s]\} \quad (15)$$

If we move from data  $n_c$  and  $n_s$  to random data  $n_c$  and  $n = n_c + n_s$ , then (15) turns into:

$$P(n_c, n | i_c, i_s) = B(n_c | n, p) \times P_{\Delta}(n | i_{\Delta}) \quad (16)$$

where  $P_{\Delta}(n | i_{\Delta})$  as well as (12) is the Poisson probability distribution with the parameter  $i_{\Delta} = [\sigma_c i_c + \sigma_s i_s] / \sigma$ , and  $B(n_c | n, p)$  is the binomial distribution with parameters  $n$  and  $p = \sigma_c i_c / \sigma i_{\Delta}$ :

$$B(n_c | n, p) = \frac{n!}{n_c!(n-n_c)!} p^{n_c} (1-p)^{n-n_c}, \quad (17)$$

$$P_{\Delta}(n | i_{\Delta}) = \frac{(\sigma i_{\Delta})^n}{n!} \exp\{-\sigma i_{\Delta}\}.$$

For a complete statistical description of the RF data, it is necessary to select an a priori model of the intensities  $i_c$  and  $i_s$ . In this regard, let us assume that the marginal distributions of both intensities are given by the same density  $\wp(i)$ . As for their joint distribution, we will assume that two cases are possible. In the first case, both intensities are completely statistically dependent due to their coincidence  $i_c = i_s$ , so their joint distribution is  $\delta(i_c - i_s) \wp(i_s) = \delta(i_s - i_c) \wp(i_c)$ , where  $\delta(i)$  is Dirac delta-function. In the second case, they are completely statistically independent, and their joint distribution is  $\wp(i_c) \wp(i_s)$ . Formally, denoting the first case of complete dependence as the 0-hypothesis  $H_0$ , and the second one as its alternative  $\bar{H}_0$ , we can

write the *a priori* (conditional in relation to  $H \in \{H_0, \overline{H}_0\}$ ) distribution of  $i_c$  and  $i_s$  in the form:

$$\rho_a(i_c, i_s | H) = \begin{cases} \delta(i_s - i_c) \wp(i_c), & H = H_0, \\ \wp(i_c) \wp(i_s), & H = \overline{H}_0. \end{cases} \quad (18)$$

Combining (16) and (18), we obtain the following distributions for the full statistical (generative) model

$$\begin{aligned} & \rho(n_c, n, i_c, i_s | H) = \\ & = P(n_c, n | i_c, i_s) \rho_a(i_c, i_s | H) = \\ & = \begin{cases} B(n_c | n, p_0) P_\Delta(n | i_c) \delta(i_s - i_c) \wp(i_c), & H = H_0; \\ P_c(n_c | i_c) P_s(n_s | i_s) \wp(i_c) \wp(i_s), & H = \overline{H}_0; \end{cases} \end{aligned} \quad (19)$$

where due to  $i_\Delta = i_s = i_c$  in the first line of the curly brace in (19) the parameter  $i_\Delta$  in  $P_\Delta(n | i_\Delta)$  (17) is replaced by  $i_c$  and the parameter  $p$  in  $B(n_c | n, p)$  (17) is replaced by  $p_0 = \sigma_c/\sigma$ . In the second line of the curly brace in (19) the original representation (15) is used for  $P(n_c, n | i_c, i_s)$ .

Marginalizing (19) we can find the unconditional distribution  $P(n_c, n | H)$  of random  $n_c$  and  $n$ . After a number of simplifications and approximations (see (Antsiperov, 2023)), it can be approximated by the following large-counts distribution:

$$\begin{aligned} & P(n_c, n | H) \approx \\ & \approx \begin{cases} B(n_c | n, p_0) \frac{1}{\sigma} \wp\left(\frac{n}{\sigma}\right), & H = H_0, \\ \frac{1}{\sigma_c} \wp\left(\frac{n_c}{\sigma_c}\right) \frac{1}{\sigma_s} \wp\left(\frac{n-n_c}{\sigma_s}\right), & H = \overline{H}_0. \end{cases} \end{aligned} \quad (20)$$

Using (20), we can introduce the likelihood ratio of the hypotheses  $H_0/\overline{H}_0$  for given data  $n_c, n$ :

$$\begin{aligned} & L(n_c, n) = \frac{P(n_c, n | H_0)}{P(n_c, n | \overline{H}_0)} = \\ & = \frac{\sigma_c \sigma_s}{\sigma} \frac{\wp\left(\frac{n}{\sigma}\right)}{\wp\left(\frac{n_c}{\sigma_c}\right) \wp\left(\frac{n-n_c}{\sigma_s}\right)} B(n_c | n, p_0) \end{aligned} \quad (21)$$

The likelihood ratio  $L(n_c, n)$  (21) can be made more interpretable by moving from the variables  $n_c, n$  to  $\delta = n/\sigma - n_c/\sigma_c$  and  $n$ . For these variables the binomial distribution admits a Gaussian approximation (for large  $n$ ). Also replacing  $\wp(n_c/\sigma_c)$  and  $\wp((n-n_c)/\sigma_s) = \wp(n_s/\sigma_s)$  in (21) by  $\wp(n/\sigma)$ , we get a simplified expression for the likelihood ratio:

$$\begin{aligned} & L(\delta, n) = \\ & = \frac{1}{\sqrt{2\pi n}} \sqrt{\frac{\sigma_c \sigma_s}{\sigma^2}} \frac{1}{\sigma} \wp\left(\frac{n}{\sigma}\right) \exp\left\{-\frac{\sigma^2 \delta^2}{2n\sigma_s/\sigma_c}\right\}. \end{aligned} \quad (22)$$

Basing on the likelihood ratio (22), one can use the uniformly most powerful unbiased test (Young, 2005) to compare the degree of agreement between hypotheses  $H_0/\overline{H}_0$  to the available data  $\delta, n$ . Namely,

according to the Neyman–Pearson criterion, one should accept  $H_0$  – the hypothesis of the coincidence  $i_\Delta = i_s = i_c$ , if  $L(\delta, n) > K_\alpha$  and reject  $H_0$ , implying  $\overline{H}_0$  – the hypothesis of a significant difference between  $i_\Delta$  and  $i_c$ , otherwise. The threshold  $K_\alpha$  clearly indicates its dependence on  $\alpha$  – the size of the test. The test size, in its turn, can be defined as the probability of  $\delta, n$  falling into the critical region  $C_\alpha = \{\delta, n | L(\delta, n) < K_\alpha\}$ , or  $\alpha = \sum_{\delta, n \in C_\alpha} \rho(\delta, n | H_0)$ , where  $\rho(\delta, n | H_0)$  is given by the first line of the curly brace (20). Having performed all the summations (integrations), one can arrive at the following explicit form of the the critical region  $C_\alpha$ :

$$C_\alpha: \frac{\sigma^2 \delta^2}{2n\sigma_s/\sigma_c} > \ln\left(\sqrt{\frac{\sigma_c \sigma_s}{2\pi n \sigma^2}} / K_\alpha \frac{1}{\sigma} \wp\left(\frac{n}{\sigma}\right)\right). \quad (23)$$

The right side of (23) can be simplified if we approximate *a priori* distribution  $\wp(i)$  by the value  $\mathcal{R}^{-1}$  on its characteristic scale  $\mathcal{R}$ . As the *a priori* average of the number of counts on the RF is approximately  $n \sim \sigma \mathcal{R}$ , we can replace  $\wp(n/\sigma)$  by  $\mathcal{R}^{-1}$  and  $n$  by  $\sigma \mathcal{R}$  in the right-hand side of (23). Thus it will turn into a constant, which we denote by  $D_\alpha^2$ :

$$\begin{aligned} & D_\alpha^2 = \ln\left(\frac{1}{K_\alpha} \sqrt{\frac{\sigma_c \sigma_s}{\pi \sigma^2}} \sqrt{2\overline{n}_a}\right) = \\ & = \frac{1}{2} \ln\left(\frac{\sigma_c \sigma_s}{2\pi \sigma^2}\right) + \frac{1}{2} \ln(\sigma \mathcal{R}) - \ln(K_\alpha) \end{aligned} \quad (24)$$

From (23,24) the size of the test  $\alpha$  takes the form:

$$\alpha = \frac{2}{\sqrt{\pi}} \int_{D_\alpha}^{\infty} \exp\{-\xi^2\} d\xi \sum_{n=0}^{\infty} \frac{1}{\sigma} \wp\left(\frac{n}{\sigma}\right) = \text{erfc}(D_\alpha) \quad (25)$$

where it is taken into account that  $\sum_{n=0}^{\infty} \frac{1}{\sigma} \wp\left(\frac{n}{\sigma}\right) \approx \int_0^{\infty} \wp(i) di = 1$  and the standard complementary error function  $\text{erfc}(x)$  is used. Relation (25) implicitly relates  $\alpha$  and  $D_\alpha$  and thus there is no need to find the threshold  $K_\alpha$ , when  $\alpha$  is given. In accordance with (25),  $D_\alpha$  can be calculated directly from  $\alpha$  as an inverse error function  $\text{erf}^{-1}(1 - \alpha)$ . After  $D_\alpha$  is fixed, the criterion for rejecting the hypothesis  $H_0$  – the hypothesis of the coincidence  $i_\Delta = i_s = i_c$  (i.e. accepting alternative  $\overline{H}_0$  of intensity jump of on RF) takes the following final form:

$$\delta^2 > \frac{2n\sigma_s/\sigma_c}{\sigma^2} D_\alpha^2 \leftrightarrow |\delta| > \sqrt{2 \frac{\sigma_s}{\sigma_c} \frac{D_\alpha}{\sigma}} \sqrt{n}. \quad (26)$$

Returning to the original formulation of our method for detecting edges using zero-crossing lines, set out in the first section, we note the following here. The unbiased estimates of the average intensities  $i_c$ ,  $i_s$  (14) and  $i_\Delta$  (16) can be given by the RF registered data  $n_c/\sigma_c$ ,  $n_s/\sigma_s$  and  $n/\sigma$ . By definition of a

random variable  $\delta = n/\sigma - n_c/\sigma_c$  specifies an unbiased estimate of the value  $i_\Delta - i_c$ . But, in view of the proportionality  $i(\vec{x}) = \beta I(\vec{x})$ , we have relations  $i_c = \beta \bar{I}_c$ ,  $i_s = \beta \bar{I}_s$  and  $i_\Delta = \beta \bar{I}$ . Therefore,  $\delta$  is an unbiased estimate of  $\beta(\bar{I} - \bar{I}_c) = \beta \delta \bar{I}$ . Thus, zero-crossing lines of  $\delta \bar{I}$  will also be zero-crossing lines also of  $\delta$  and the edge detection algorithm can literally be reformulated in terms of the data  $\{\delta(\vec{X}_i)\}$  over all receptive fields. In this case, ON-fields are determined by the positive condition on the right side of (30), and OFF-fields by the negative. Moreover, since the thresholds in these conditions depend on  $\sqrt{n}$ , data  $\{n(\vec{X}_i)\}$  are also needed for all fields.

Finally, the formulation of the proposed edge detection method in terms of RF data  $\{\delta_i, n_i\}$ ,  $\delta_i = \delta(\vec{X}_i)$ ,  $n_i = n(\vec{X}_i)$  has the form:

Step 1. For all receptive fields in positions  $\{\vec{X}_i\}$  find, basing on sampling representation  $S_k = \{\vec{x}_j\}$ , the numbers of counts  $n_{ci}$  in the centres,  $n_{si}$  – in the surrounds and  $n_i = n_{ci} + n_{si}$  in the RF regions. Using them, generate sufficient data  $\{\delta_i, n_i\}$ :

$$\delta_i = n_i/\sigma_i - n_{ci}/\sigma_{ci} \text{ and } n_i.$$

Step 2. Basing on the data  $\{\delta_i, n_i\}$  build the classes of ON- and OFF-fields:

$$\delta_i > \sqrt{2 \frac{\sigma_{si} D_\alpha}{\sigma_{ci} \sigma_i}} \sqrt{n_i} \rightarrow \text{ON - field};$$

$$\delta_i < -\sqrt{2 \frac{\sigma_{si} D_\alpha}{\sigma_{ci} \sigma_i}} \sqrt{n_i} \rightarrow \text{OFF - field};$$

Step 3. For all pairs of nearest ON- and OFF-fields find on the connecting their centres segments  $\vec{X}_k \leftrightarrow \vec{X}_l$ , using  $\delta_k \leftrightarrow \delta_l$  interpolation, zero-points  $\vec{X}_{kl}$ , see Figure 2.

Step 4. Connect all found nearest zero points  $\{\vec{X}_{kl}\}$  with a broken line, thereby obtaining an approximation of the desired zero-crossing line, see Figure 2.

Note that in Step 2, not all the fields will be classified as ON- or OFF-fields. Moreover, practice shows that usually their number is noticeably less than the number of all fields. This, by the way, gives reason to call the method proposed an algorithm for encoding a sample representation  $S_k = \{\vec{x}_j\}$ , see in this regard (Antsiperov, 2023). Moreover, if the factor  $2\sigma_s/\sigma_c$  in the test thresholds of Step 2 is of the order of one, the tests can be reformulated as  $v_i > D_\alpha \sqrt{n_i}$  and  $v_i < -D_\alpha \sqrt{n_i}$ , where the counts difference  $v_i = \sigma_i \delta_i = n_i - \hat{n}_i$ , and  $\hat{n}_i = \sigma_i n_{ci}/\sigma_{ci}$  represents centre-corrected estimates of the total number of counts on the RF.

## 4 NEUROMORPHIC DECODING (INTERPOLATION) OF RF ENCODED DATA

To illustrate the capabilities of the method proposed, we present below the results of image edge-directed interpolation, based on the data  $\{\delta_i, n_i\}$  generated by Figure 3 (right) sampling representation. To restore (decoding) encoded images, the reconstruction area, like the area of the original image  $\Omega$ , is covered with a similar (in number, shape, and arrangement of fields) RF system. For example, a RF system consisting of 900 square fields, shown in Figure 4, was used for encoding / restoration of the image and its sampling representation, presented in Figure 3.

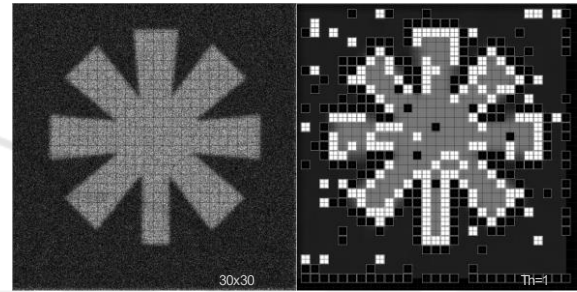


Figure 4: The result of RF encoding of image sampling representation shown in Figure 3. On the left is a sampling representation with a grid of  $30 \times 30$  receptive fields, on the right are RFs with a censored code  $v_i$ : white – ON-RFs with  $v_i > D_\alpha \sqrt{n_i}$ , black – OFF-RFs with  $v_i < -D_\alpha \sqrt{n_i}$ .

Using this auxiliary RF system, a grid dual to it is constructed, the nodes of which are the centres of the corresponding RFs, and the edges are the segments connecting the nearest nodes. To each  $i$ -th node the data (code)  $\{v_i, n_i\}$  of the  $i$ -th RF is also assigned.

Classical bilinear image interpolation can be constructed only from the “smooth” part of the code  $\{n_i\}$ . Namely, the  $n_i$  values are first interpolated along the vertical edges of the grid, and then linearly along all rows of all cells based on the already interpolated vertical edges. The interpolation we propose also uses two-pass reconstruction. During the first pass, the  $n_i$  values are also interpolated along the grid edges, not only vertical, but also horizontal. What’s important here is that this interpolation is not necessarily linear. If at the nodes of a given edge the values  $v_i$  and  $v_j$  are nonzero and have different signs, then such an edge is considered as intersecting the zero-crossing line – the line of contrast difference, and the middle of the edge is taken as the intersection (zero-) point. The interpolation in this case is piecewise constant on both sides of this edge. In the



second pass, the values in the grid cells are linearly interpolated from the values on their edges. Moreover, if a pair of cell edges intersects with the zero-crossing line, then interpolation is carried out along a segment connecting the zero-points. If not, then interpolation is performed along the rows of cells, as in classical interpolation. The results of both types of interpolation are presented in Figure 5.

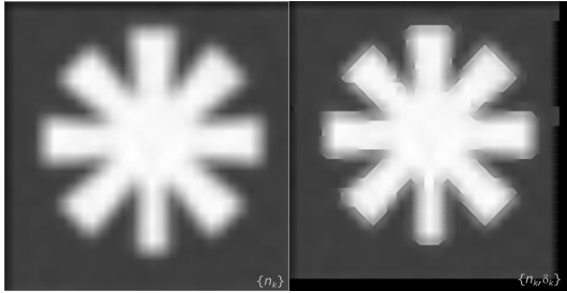


Figure 5: Interpolation based on the codes of Figure 4, generated from the image of Figure 3. On the left – bilinear interpolation of the image based only on the “smooth” part  $\{n_i\}$  of the code, on the right – interpolation of the image along the zero-crossing line segments, specified also by the “details”  $\{v_i\}$ .

## 5 CONCLUSIONS

A special feature of the proposed method is the concept of receptive fields, widely used in its context. The use of the RF structure allows one to effectively overcome the known difficulties of numerical algorithms that process mixtures with a large number of components. This conclusion follows, among other things, from the existing experience in computer implementation of the method: all illustrative materials presented in the work were obtained as part of computational experiments. Experiments confirmed the effectiveness of the method in terms of memory resources / computation time. For example, the encoding / reconstruction of 1000x1000 pixels, 8 bits colour depth image, presented in this work as an illustration (see Figures 3, 4, 5), required a calculation time of only a few milliseconds even in the case of the densest grid of 150x150 nodes (22500 components).

In general, based on the results obtained, it seems reasonable to express the hope that the approach proposed in the work will find soon both further theoretical development and fruitful use in applied problems.

## REFERENCES

- Allebach, J., Wong, P.W. (1996). Edge-directed interpolation. In *Proceeding of the 3rd IEEE Int. Conference on Image Processing*, V. 2, P. 707–710. doi: 10.1109/icip.1996.560768.
- Antsiperov V. E. (2022). Generative Model of Autoencoders Self-Learning on Images Represented by Count Samples. In *Automation and Remote Control*. V. 83 (12), P. 1959-1983. doi: 10.1134/S00051179220120098.
- Antsiperov, V., Kershner, V. (2023). Retinotopic Image Encoding by Samples of Counts. In *Pattern Recognition Applications and Methods. ICPRAM 2021 2022, De Marsico, M., Sanniti di Baja, G., Fred, A. (eds). Lecture Notes in Computer Science*, V. 13822. Springer, Cham. doi: 10.1007/978-3-031-24538-1\_3.
- Antsiperov V. (2023) New Centre/Surround Retinex-like Method for Low-Count Image Reconstruction. In *Proceedings of the 12th International Conference on Pattern Recognition Applications and Methods (ICPRAM 2023)*, SCITEPRESS – Science and Technology Publications, Lda, P. 517-528. doi: 10.5220/0011792800003411.
- Barrett, H., White, T., Parra, L. (1997). List-mode likelihood. In *J. Opt. Soc. Am. A*, V. 14, P. 2914–2923. doi:10.1364/JOSAA.14.002914.
- Bear M. F., Connors B. W., Paradiso M. A. (2007). The eye. In *Neuroscience: Exploring the Brain*, P. 277–307.
- Christensen D. V., et al. (2022). 2022 roadmap on neuromorphic computing and engineering. In *Neuromorphic Computing and Engineering*. V. 2, P. 022501. doi: 10.1088/2634-4386/ac4a83.
- Haralick, R. M. (1984). Digital Step Edges from Zero Crossing of Second Directional Derivatives. In *IEEE Transactions on Pattern Analysis and Machine Intelligence*, PAMI-6(1), P. 58–68. doi:10.1109/tpami.1984.4767475.
- Kuffler S. W. (1953). Discharge patterns and functional organization of mammalian retina. In *Journal of neurophysiology*, V. 16(1), P. 37–68. doi: 10.1152/jn.1953.16.1.37
- Land E. H. (1977). The Retinex theory of color vision. In *Scientific American*, V. 237(6), P. 108–129. doi: 10.1038/scientificamerican1277-108
- Marr, D., Hildreth, E. (1980) Theory of Edge Detection. In *Proceedings of the Royal Society of London. Series B, Biological Sciences*, V. 207(1167), P. 187–217.
- Nguyen G., et al. (2019) Machine learning and deep learning frameworks and libraries for large-scale data mining: a survey. In *Artificial Intelligence Review*. V. 52, P. 77–124. doi: 10.1007/s10462-018-09679-z.
- Young G. A., Smith R. L. (2005). *Essentials of statistical inference*. Cambridge University Press. Cambridge.